Blue Self-Frequency Shift of Slow Solitons and Radiation Locking in a Line-Defect Waveguide

P. Colman,[1] S. Combrié,[1] G. Lehoucq,[1] A. de Rossi,[1] and S. Trillo[2,*]

[1]*Thales Research and Technology France Campus Polytechnique, 1, Avenue Augustin Fresnel, 91767 Palaiseau cedex, France*
[2]*Department of Engineering, University of Ferrara, Via Saragat 1, 44122 Ferrara, Italy*

(Received 3 March 2012; published 28 August 2012)

We investigate experimentally resonant radiation processes driven by slow solitons in a dispersion-engineered photonic crystal waveguide in a regime virtually free of dissipative nonlinear processes (two-photon absorption and Raman scattering). Strong (30% energy conversion) Cherenkov-like radiation accompanied by the blue self-frequency shift of the soliton is observed close to the zero dispersion point, and is explained in terms of the soliton-radiation locking of the velocity.

DOI: 10.1103/PhysRevLett.109.093901 PACS numbers: 42.65.Tg, 42.65.Wi, 42.70.Nq, 42.70.Qs

The interest in optical temporal solitons originates from their nearly ideal behavior as information carriers in both long-haul fiber transmission [1] and resonators [2]. However, as has emerged in the last decade, solitons are also crucial to understanding highly dynamical phenomena which involve the strong spectral redistribution of energy, observed in different settings such as silica photonic crystal fibers (PCF) [3–9], highly nonlinear nanowires [10], or quadratic materials [11]. The most dramatic of such phenomena, supercontinuum generation in PCF, is affected by solitons through concurrent mechanisms such as the Raman induced soliton self-frequency shift (SSFS) [12,13], fission [4], four-wave mixing [14], and resonant (Cherenkov-like) radiation [9]. In this case spectral broadening extends across the zero of the group-velocity dispersion (GVD). In particular, broadening over red wavelengths where the GVD is anomalous is mainly affected by the Raman red SSFS [12,13], whereas on the blueshift side where the GVD becomes normal, spectral broadening is mediated by the resonant amplification of linear dispersive waves. Such a radiative mechanism ideally occurs at frequencies determined by the underlying mechanism of resonance between the soliton (in the anomalous GVD region) and linear waves (in the normal GVD region), driven by higher-order dispersive terms [15,16]. However, only when interacting with the soliton beyond this simple resonant mechanism does the radiation become prominent. In particular, in silica PCF, a mechanism for trapping the radiation has been discovered (usually observed with meters of PCF and KW power levels), where an essential role is played by soliton deceleration (also a consequence of Raman SSFS [6–9]).

In this Letter we report the observation of resonant radiation in a different setting, namely a line-defect photonic crystal waveguide (PhC-WG) in a ternary semiconductor (GaInP) slab. Recently such types of waveguides have been successfully employed to demonstrate temporal soliton compression [17]. Here, by exploiting a novel PhC-WG sample with dispersion tailored to work close to the first zero of a double-zero GVD profile, we are able to demonstrate efficient emission of dispersive waves in resonance with the soliton. Our system exploits the slow-light enhancement of the Kerr response [17–19], which, along with the fact that the system exhibits no Raman scattering and is virtually free of nonlinear absorption, makes a nearly ideal environment for studying the interaction between the soliton and dispersive waves. Moreover, due to the dispersive features of our guide the radiation turns out to be redshifted. This causes the soliton to shift toward high frequencies owing to a pure recoil phenomenon [16], which represents a new mechanism compared with recent observations where the soliton blueshift in PCF results from the variation of the zero GVD wavelength along the fiber in tapered solid-core PCF [20], or from photoionization processes in hollow-core PCF filled with a Raman-inactive noble gas [21,22]. While the net blueshift in our arrangement is smaller compared with that achieved in PCF, our system involves length (mm), power (W), and temporal (ps) scales which compare favorably with all other systems studied so far, making the phenomenon compatible with on-chip applications pumped by compact semiconductor laser sources.

The measurements have been performed on a 190-nm thick GaInP membrane which is patterned with a triangular lattice of air holes with period $a = 470$ nm and nominal radius 105 nm ($r = 0.22a$). A missing line of holes constitutes the PhC-WG, whose dispersion is engineered in such a way as to present two zeros of the GVD [see Fig. 1(a)]. This is obtained by the weak coupling of the fundamental even and odd modes by slightly shifting the two innermost lines of holes in opposite longitudinal directions (part of a more general strategy to control dispersion properties [23]).

In Fig. 1 we report the measured dispersion, i.e., the dependence of the group index [Fig. 1(b)] and GVD [Fig. 1(a)] on wavelength. As shown, the GVD vanishes at $\lambda_0 = 1551.3$ nm, separating the anomalous ($\lambda < \lambda_0$) from the normal GVD ($\lambda > \lambda_0$) regimes. Unless stated otherwise, the input wavelength λ will be henceforth referred to λ_0 by introducing the detuning $\delta\lambda = \lambda - \lambda_0$. The waveguide is $L = 1.5$ mm long and the use of mode

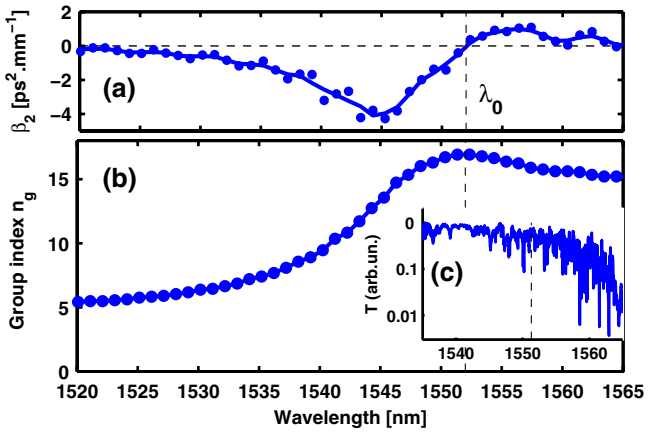

FIG. 1 (color online). PhC-WG dispersion: (a) GVD vs wavelength; (b) group index $n_g(\lambda)$. Inset (c): transmission spectrum. λ_0 indicates the first zero of the GVD.

matching tapers [24] reduces the input-output coupling losses to about 2 dB/facet which, along with losses due to coupling objectives (4 dB), results in an overall transmission of about 2% at λ_0. The effective length $1/\alpha = 4.34/\alpha$ [dB/mm] associated with linear losses in the PhC-WG ranges from 4 to 0.8 mm (at λ_0), and, being much longer than the nonlinear length, enables adiabatic pulse evolution as long as we operate in the vicinity of the first zero of the GVD. Here the redshifted radiation is efficiently observed in spite of the higher losses in the long wavelength region [see Fig. 1(c)]. Conversely, close to the second zero of the GVD, the PhC-WG becomes too lossy to detect any dynamics. Importantly, the nonlinear losses have also been minimized since GaInP does not present, thanks to its large gap of 1.9 eV, any two-photon absorption (TPA) around 1.55 μm (i.e., $\hbar\omega = 0.8$ eV) at variance with, e.g., GaAs and silicon. The purpose of using a TPA-free material is (i) to increase the nonlinear absorption threshold to achieve larger powers in the waveguide and (ii) to avoid the strong generation of free carriers which can screen the fast electronic nonlinearities through the absorption and dispersion of free carriers. The residual three-photon absorption affects only slightly the dynamics since we operate below its threshold (input power $\simeq$ 10 W). Stimulated Raman scattering is also absent because its estimated peak ($\sim$ 14 THz) is well above the PhC-WG bandwidth ($\sim$ 10 THz).

In our experiment we launch along the sample laser pulses of 1.8 ps (FWHM) with tunable wavelength and adjustable power, and record the output spectra for increasing input peak powers. Figure 2(a) shows the typical output spectra (log scale), which are recorded for an input detuning $\delta\lambda = -4.8$ nm. As shown, at low power the spectrum exhibits a monotonic decay across the zero GVD point, closely following the reference (input) pulse spectrum which turns out to be slightly broadened due to a residual chirp. At higher powers, this tail in the normal GVD

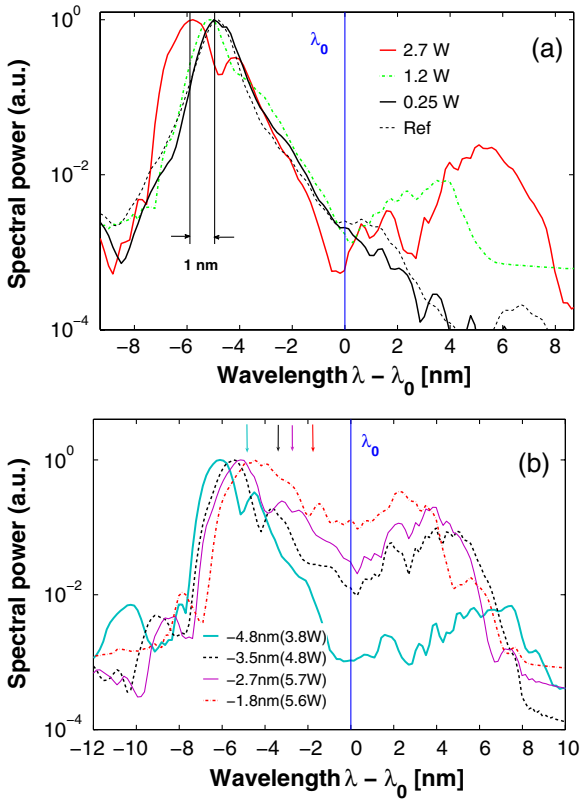

FIG. 2 (color online). (a) Output spectra (log scale) for different input peak powers, when the input pulse is detuned by $\delta\lambda = -4.8$ nm (a SSFS of -1 nm is indicated). (b) Output spectra observed for different input detunings $\delta\lambda$ (the spectra are recorded after tuning the laser and hence correspond to slightly different powers, as indicated). The arrows locate the input wavelengths.

regime acts as a seed to be amplified (at the expense of soliton energy), according to the mechanism of resonant enhancement of linear waves, owing to phase matching with the soliton [see also Eq. (2) below], first predicted for standard telecom fibers by Wai *et al.* [15]. Here, however, the situation is opposite with respect to both standard fibers and PCF, with the radiation being expected at longer (red) wavelengths where the GVD is normal [see Fig. 1(a)]. Such a redshifted radiation peak clearly emerges in the experiment [see Fig. 2(a)], when the peak power is raised above $P_c \simeq 1$ W, and becomes even stronger at larger powers (see curve for $P_c = 2.7$ W). Importantly, we clearly observe that the radiation has a backaction on the soliton inducing a blue SSFS of nearly 1 nm. This is due to a pure recoil mechanism [16] since, in the absence of the radiation, no shift is detected [17]. We point out that the dispersive wave is efficiently generated when the power is such that we operate with soliton numbers $N = \sqrt{L_d/L_{\rm nl}} > 1$. In the PhC-WG the effective Kerr coefficient γ depends on the group index which determines the enhancement factor (see Ref. [25] for a detailed

discussion, and the Supplemental Material [17]). For the relatively large detuning of Fig. 2(a), we estimate, using a material Kerr index $n_{2I} = 0.57 \times 10^{-7}$ m^2/W, a coefficient $\gamma \simeq 1010$ (Wm)$^{-1}$, which gives a nonlinear length $L_{\rm nl} = (\gamma P_c)^{-1} \simeq 360$ μm at power $P_c = 2.7$ W. Given the dispersion length $L_d \simeq 0.58$ mm, this corresponds to a soliton number $N \sim 1.3$.

Clearly the output spectra are also sensitive to the input wavelength, due to the dispersive features illustrated in Fig. 1. Spectra taken at higher powers for different input detunings $\delta\lambda$ are compared in Fig. 2(b). As shown, the dispersive wave peak is clearly visible at all detunings and grows as the input wavelength is tuned closer to λ_0. In order to show that we observe, indeed, an even stronger soliton recoil at smaller detunings, we show in Fig. 3 the spectra (linear scale) recorded for $\delta\lambda = -1.8$ nm, and increasing powers. As shown, in this case, a blue SSFS of $\sim$2.5 nm is observed at a power level $P_c \simeq 5.6$ W ($L_{\rm nl} \simeq 120$ μm, $L_d \simeq 2$ mm, $N \simeq 4$). When the detuning is reduced even further up to a few tenths of a nanometer, the output spectrum turns out to be strongly broadened without a distinguishable radiation peak.

The data reported in Figs. 2 and 3 show, importantly, that the dispersive wave turns out to be quite strong, weighting up to 30% of the soliton energy after only 1.5 mm of propagation. This cannot be explained solely in terms of the soliton-radiation resonance mechanism which, while being able to correctly capture the frequency of the splitting wave (see below), predicts a dispersive wave that remains exponentially small (at all orders of asymptotic expansions, as shown in Ref. [15]). In order to explore why it is not so in our setting, we have performed a careful simulation of the propagation complemented by the analysis of the resonance condition. We model the propagation by means of the following generalized nonlinear Schrödinger equation for the temporal envelope $E(z, t)$

$$i\frac{\partial E}{\partial z} + D(i\partial_t)E + \gamma|E|^2E = -i\frac{\alpha}{2}E - i\alpha_3|E|^4E, \quad (1)$$

where $\alpha(\omega)$ and $\alpha_3(\omega)$ are the linear and nonlinear loss coefficients, respectively. We find that the latter ($\alpha_3 \simeq 10$ W^{-2}m^{-1} at λ_0) has a minor impact for the values of powers considered here. The dispersion operator $D(i\partial_t) = \sum_{n\geq 2}\partial_\omega^n k(i\partial_t)^n/n!$ accounts for dispersion at all orders, with t being the retarded time in the moving frame at velocity c/n_g (calculated at the input wavelength). Here we use a polynomial interpolation of the data shown in Fig. 1(a). The outcome of a typical simulation (extended up to $z = 3$ mm), obtained for an input detuning $\delta\lambda = -3.4$ and an unchirped sech-shaped input ($P_c = 2.8$ W, FWHM 1.8 ps), is displayed in Fig. 4. In Fig. 4(a) the initial spectral broadening that stems from temporal compression (here $N \simeq 1.5$) turns into an emission of radiation at the activation length where the maximum peak power is reached ($z \sim 1$ mm). As the radiation grows, the momentum conservation, which we verified to be approximately satisfied due to the modest impact of losses, is responsible for the observed soliton blueshift (soliton recoil). Then no significant further changes are detected beyond the PhC-WG length. Temporally the dispersive wave is ahead of the soliton being emitted along the leading edge of the pulse (data not shown). However, the radiation is slower at the frequency where it builds up, owing to a higher n_g (see also Fig. 5). Furthermore, the soliton frequency is blueshifted

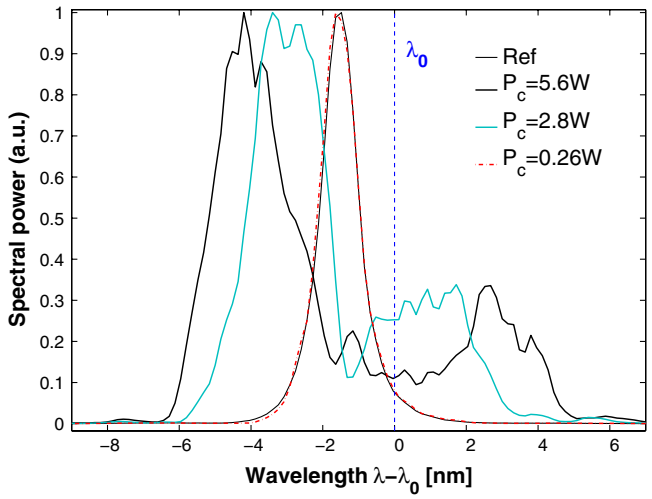

FIG. 3 (color online). Output spectrum (linear scale) for an input detuning $\delta\lambda = -1.8$ nm, showing strong soliton recoil with increasing power.

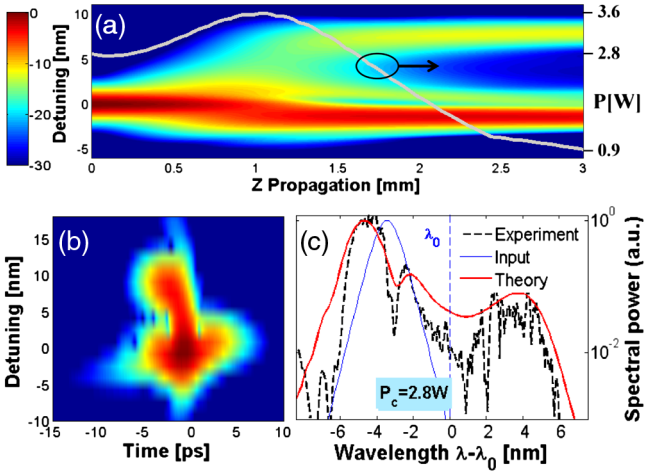

FIG. 4 (color online). (a) Color map of spectrum evolution from Eq. (1) with $P_c = 2.8$ W, $\delta\lambda = -3.4$, over 3 mm (twice the PhC-WG length). Here detuning is referred to the input wavelength. The gray curve gives the peak power vs z. (b) Simulated spectrogram (time-wavelength map) at PhC-WG output ($z = 1.5$ mm). A Blackman sliding window is used to avoid spurious oscillations in the spectrum. (c) Comparison between experimental and simulated (at $z = 1.5$ mm) spectra. The blue curve is the numerical input.

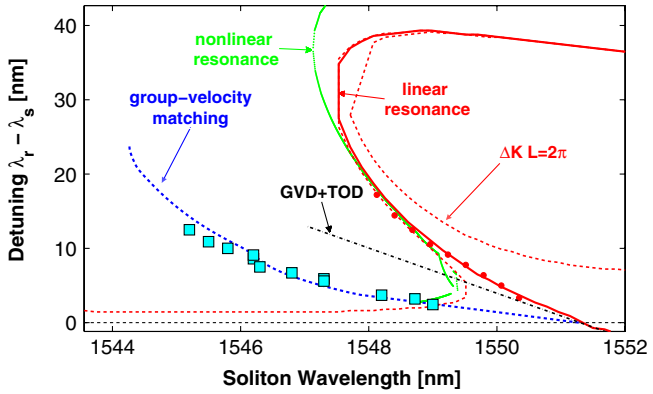

FIG. 5 (color online). Radiation-soliton detuning vs soliton wavelength. The linear resonance curve ($k_{\rm nl} = 0$, thick red curve and dots calculated using the interpolated dispersion, and the measured values, respectively) is compared with the limit arising from GVD + TOD (dot-dashed line), and with the nonlinear resonance curve ($k_{\rm nl} \neq 0$) corresponding to $P_c = 6$ W. For completeness linear mismatch curves corresponding to 2π over L are also reported (dashed). The squares (cyan) are the detunings measured at the waveguide output vs output soliton wavelength. The blue dashed line indicates group velocity matching.

due to the recoil mechanism and hence accelerated (n_g decreases), until eventually the soliton catches up and travels locked with the dispersive wave, which might explain why the radiative process is so efficient. In order to show that the radiation remains indeed locked to the pulse in the anomalous GVD regime we have also reported in Fig. 4(b) the numerical time-frequency map or spectrogram (see, e.g., Ref. [9]) corresponding to the output ($z = 1.5$). Finally, in Fig. 4(c), we compare the simulated and the measured spectra. The satisfactory agreement proves the validity of the dispersion law employed in the simulations. At higher powers ($N > 2$), the simulations also show spectral branching of the dispersive wave arising from a second compression cycle of the soliton [8], which, however, could not be probed experimentally in our sample since it occurs for $z > 1.5$ mm.

In order to get further insight into the radiative mechanism, we have analyzed the resonance condition between the soliton and the radiation (at frequencies ω_s and ω_r, respectively) [4,9,16]:

$$\sum_{n\geq 2} \partial_\omega^n k|_{\omega_s} \frac{(\omega_r - \omega_s)^n}{n!} = k_{\rm nl}, \qquad (2)$$

which can be obtained from the phase-matching constraint $k(\omega_r) - k(\omega_s) - (\omega_r - \omega_s)/V_s = k_{\rm nl}$, by expanding $k(\omega_r)$ around ω_s. Here $k(\omega)$ is the dispersion law, V_s is the soliton velocity, and $k_{\rm nl} = \gamma P_c/2$ is the nonlinear phase shift. The detunings $\lambda_r - \lambda_s$ which fulfill Eq. (2), calculated by employing the dispersion law used in Eq. (1), are displayed in Fig. 5 as a function of the soliton wavelength. First, we notice that the nonlinear correction $k_{\rm nl}$ has a small impact, as one can clearly see by comparing the linear ($k_{\rm nl} = 0$) and nonlinear ($k_{\rm nl} \neq 0$, $P_c = 6$ W) resonance curves, which remain very close, except for λ_s in close proximity to λ_0. Conversely, higher-order dispersion is important since the linear resonance condition deviates significantly from the condition $\delta\omega = 3|\partial_\omega^2 k|/\partial_\omega^3 k$ characteristic of truncation to third-order dispersion (TOD) [15]. Much more importantly, however, by reporting (see cyan squares) the measured detuning of the radiation (referred to the output soliton frequency) taken from different spectra recorded at high powers ($P_c = 2.5$–5 W), we can clearly see that the data significantly deviate from the resonance curves based on Eq. (2). Rather, they closely match the curve characteristic of soliton-radiation group-velocity matching (dashed blue curve in Fig. 5). This gives an additional indication of the fact that the radiation tends to travel locked in time to the soliton, contributing to making the net energy transfer particularly efficient.

In conclusion, we have observed efficient emission from ps pulses of redshifted resonant radiation in a millimeter-long dispersion-engineered PhC-WG, working in the moderate slow-light regime and in the absence of nonlinear scattering and absorption. Large broadening (~ 2 THz, ten times the input bandwidth) along with the blueshift of the soliton is observed, constituting a significant step forward towards the management of on-chip broadband sources compatible with compact semiconductor pump lasers.

This work has been supported by the Seventh Framework Programme of the European Commission through the GOSPEL and COPERNICUS projects.

*alfredo.derossi@thalesgroup.com

[1] Y. Kodama and A. Hasegawa, *Solitons in Optical Communications* (Clarendon, Oxford, 1995).
[2] F. Leo, S. Coen, P. Kockaert, S.-P. Gorza, P. Emplit, and M. Haelterman, Nature Photon. **4**, 471 (2010).
[3] J. K. Ranka, R. S. Windeler, and A. J. Stentz, Opt. Lett. **25**, 25 (2000).
[4] A. V. Husakou and J. Herrmann, Phys. Rev. Lett. **87**, 203901 (2001).
[5] I. Cristiani, R. Tediosi, L. Tartara, and V. Degiorgio, Opt. Express **12**, 124 (2004).
[6] F. Biancalana, D. V. Skryabin, and A. V. Yulin, Phys. Rev. E **70**, 016615 (2004); D. V. Skryabin, F. Luan, J. C. Knight, and P. St. J. Russell, Science **301**, 1705 (2003); A. V. Gorbach and D. V. Skryabin, Nature Photon. **1**, 653 (2007).
[7] J. M. Dudley, G. Genty, and S. Coen, Rev. Mod. Phys. **78**, 1135 (2006).
[8] T. X. Tran and F. Biancalana, Phys. Rev. A **79**, 065802 (2009).
[9] D. V. Skryabin and A. V. Gorbach, Rev. Mod. Phys. **82**, 1287 (2010).
[10] D. I. Yeom, E. C. Mägi, M. R. E. Lamont, M. A. F. Roelens, F. Libin, and B. J. Eggleton, Opt. Lett. **33**, 660 (2008); M. Lamont, B. Luther-Davies, D.-Y. Choi, S. Madden, and B. J. Eggleton, Opt. Express **16**, 14938 (2008).

[11] M. Bache, O. Bang, B. B. Zhou, J. Moses, and F. W. Wise, Phys. Rev. A **82**, 063806 (2010).
[12] J. P. Gordon, Opt. Lett. **11**, 662 (1986).
[13] D. V. Skryabin, F. Luan, J. C. Knight, and P. St. J. Russell, Science **301**, 1705 (2003).
[14] D. V. Skryabin and A. V. Yulin, Phys. Rev. E **72**, 016619 (2005).
[15] P. K. A. Wai, C. R. Menyuk, Y. C. Lee, and H. H. Chen, Opt. Lett. **11**, 464 (1986); **12**, 628 (1987); P. K. A. Wai, H. H. Chen, and Y. C. Lee, Phys. Rev. A **41**, 426 (1990).
[16] N. Akhmediev and M. Karlsson, Phys. Rev. A **51**, 2602 (1995).
[17] P. Colman, C. Husko, S. Combrié, I. Sagnes, C. W. Wong, and A. De Rossi, Nature Photon. **4**, 862 (2010).
[18] M. Notomi, K. Yamada, A. Shinya, J. Takahashi, C. Takahashi, and I. Yokohama, Phys. Rev. Lett. **87**, 253902 (2001).
[19] H. Gersen, T. J. Karle, R. J. P. Engelen, W. Bogaerts, J. P. Korterik, N. F. van Hulst, T. F. Krauss, and L. Kuipers, Phys. Rev. Lett. **94**, 073903 (2005).
[20] S. P. Stark, A. Podlipensky, and P. St. J. Russell, Phys. Rev. Lett. **106**, 083903 (2011).
[21] N. Y. Joly, J. Nold, W. Chang, P. Hölzer, A. Nazarkin, G. K. L. Wong, F. Biancalana, and P. St. J. Russell, Phys. Rev. Lett. **106**, 203901 (2011).
[22] M. F. Saleh, W. Chang, P. Hölzer, A. Nazarkin, J. C. Travers, N. Y. Joly, P. St. J. Russell, and F. Biancalana, Phys. Rev. Lett. **107**, 203902 (2011).
[23] P. Colman, S. Combrié, G. Lehoucq, and A. De Rossi, Opt. Express **20**, 13108 (2012).
[24] Q. V. Tran, S. Combrié, P. Colman, and A. De Rossi, Appl. Phys. Lett. **95**, 061105 (2009).
[25] M. Santagiustina, C. G. Someda, G. Vadalà, S. Combrié, and A. De Rossi, Opt. Express **18**, 21024 (2010).